Predictor-corrector framework for the sequential assembly of optical systems based on wavefront sensing

CHRISTOPHER SCHINDLBECK,* CHRISTIAN PAPE, AND EDUARD REITHMEIER

Institute of Measurement and Automatic Control, Leibniz Universität Hannover, 30167 Hanover, Germany
christopher.schindlbeck@imr.uni-hannover.de

Abstract: Alignment of optical components is crucial for the assembly of optical systems to ensure their full functionality. In this paper we present a novel predictor-corrector framework for the sequential assembly of serial optical systems. Therein, we use a hybrid optical simulation model that comprises virtual and identified component positions. The hybrid model is constantly adapted throughout the assembly process with the help of nonlinear identification techniques and wavefront measurements. This enables prediction of the future wavefront at the detector plane and therefore allows for taking corrective measures accordingly during the assembly process if a user-defined tolerance on the wavefront error is violated. We present a novel notation for the so-called hybrid model and outline the work flow of the presented predictor-corrector framework. A beam expander is assembled as demonstrator for experimental verification of the framework. The optical setup consists of a laser, two bi-convex spherical lenses each mounted to a five degree-of-freedom stage to misalign and correct components, and a Shack-Hartmann sensor for wavefront measurements.

References and links

1. H. Butler, "Position control in lithographic equipment," IEEE Control. Syst. Mag. **31**, 28–47 (2011).
2. H. Grote, G. Heinzel, A. Freise, S. Gossler, B. Willke, H. Lück, H. Ward, M. M. Casey, K. A. Strain, D. Robertson *et al.*, "Alignment control of geo 600," Class. Quantum Gravity **21**, S441 (2004).
3. C. G. Prevost and J. Genest, "Dynamic alignment of a michelson interferometer using a position-sensitive device," in "Proc. of the SPIE 49th Annual Meeting," (2004), pp. 293–304.
4. S. Li, Y. Zhang, M. Gao, L. Xu, X. Wei, J. Tong, L. Jin, and S. Cheng, *A Moving Mirror Driving System of FT-IR Spectrometer for Atmospheric Analysis* (Springer, 2011), pp. 371–377.
5. D. R. Neal and J. Mansell, "Application of shack-hartmann wavefront sensors to optical system calibration and alignment," in "Proc. 2nd Int. Workshop on Adaptive Optics for Industry and Medicine," (2000), pp. 234–243.
6. R. E. Abbink, "Interferometer alignment," (2005). US Patent 6,952,266.
7. F. Acernese, P. Amico, M. Al-Shourbagy, S. Aoudia, S. Avino, D. Babusci, G. Ballardin, R. Barillé, F. Barone, L. Barsotti *et al.*, "The virgo automatic alignment system," Class. Quantum Gravity **23**, S91 (2006).
8. A. Cenko, "Automatic interferometric alignment of a free-space optical coherence tomography system," Ph.D. thesis (2011).
9. D. Kalamatianos, P. E. Wellstead, J. M. Edmunds, and P. Liatsis, "Active alignment for two-beam interferometers," Rev. Sci. Instrum. **77**, 013103 (2006).
10. E. Morrison, B. J. Meers, D. I. Robertson, and H. Ward, "Automatic alignment of optical interferometers," Appl. Opt. **33**, 5041–5049 (1994).
11. W. Shaomin, "Matrix methods in treating decentred optical systems," Opt. quantum electronics **17**, 1–14 (1985).
12. T. W. Raasch, "Propagation of aberrated wavefronts using a ray transfer matrix," J. Opt. Soc. Am. A **31**, 964–967 (2014).
13. F. Z. Adil, E. İ. Konukseven, T. Balkan, and Ö. F. Adil, "Optical alignment procedure utilizing neural networks combined with shack–hartmann wavefront sensor," Opt. Eng. **56**, 051402 (2017).
14. A. N. Das, D. O. Popa, J. Sin, and H. E. Stephanou, "Precision alignment and assembly of a fourier transform microspectrometer," J. Micro-Nano Mechatronics **5**, 15 (2009).

15. J. Sin, W. H. Lee, and H. E. Stephanou, "Sensitivity analysis of an assembled fourier transform microspectrometer," in "Proc. of SPIE Vol. 7680," (2010), p. 76800T.
16. J. Fang and D. Savransky, "Automated alignment of a reconfigurable optical system using focal-plane sensing and kalman filtering," Appl. Opt. **55**, 5967–5976 (2016).
17. D. Redding, N. Sigrist, J. Z. Lou, Y. Zhang, and P. Atcheson, "Optical state estimation using wavefront data," in "Proc. of SPIE Vol. 5523," (2004), pp. 212–224.
18. N. Patel and C. S. Narayanamurthy, "Measurement of optical misalignment using wavefront sensing," Opt. Eng. **54**, 104106 (2015).
19. V. Kalikivayi, V. C. P. Kumar, K. Kannan, and A. R. Ganesan, "Tolerance analysis of misalignment in an optical system using shack–hartmann wavefront sensor: experimental study," Opt. Eng. **54**, 075104 (2015).
20. E. D. Kim, Y.-W. Choi, M.-S. Kang, and S. C. Choi, "Reverse-optimization alignment algorithm using zernike sensitivity," J. Opt. Soc. Korea **9**, 68–73 (2005).
21. S. Kim, H.-S. Yang, Y.-W. Lee, and S.-W. Kim, "Merit function regression method for efficient alignment control of two-mirror optical systems," Opt. Express **15**, 5059–5068 (2007).
22. H.-S. Yang, S.-H. Kim, Y.-W. Lee, J.-B. Song, H.-G. Rhee, H.-Y. Lee, J.-H. Lee, I.-W. Lee, and S.-W. Kim, "Computer aided alignment using zernike coefficients," in "Proc. of SPIE Vol. 6293," (2006), p. 62930I.
23. H. Lee, G. B. Dalton, I. A. Tosh, and S.-W. Kim, "Computer-guided alignment ii: Optical system alignment using differential wavefront sampling," Opt. Express **15**, 15424–15437 (2007).
24. H.-Z. Duan, Y.-R. Liang, and H.-C. Yeh, "Analysis of non-linearity in differential wavefront sensing technique," Opt. Lett. **41**, 914–917 (2016).
25. E.-S. Oh, S. Kimc, Y. Kim, H. Lee, S.-W. Kima, and H.-S. Yang, "Integration of differential wavefront sampling with merit function regression for efficient alignment of three-mirror anastigmat optical system," in "Proc. of SPIE Vol. 7793," (2010), p. 77930F.
26. M. Holters, A. Gatej, S. Haag, T. Müller, P. Loosen, and C. Brecher, "Approach for self-optimising assembly of optical systems," Int. J. Comput. Integr. Manuf. **29**, 1227–1237 (2016).
27. L. M. Rios and N. V. Sahinidis, "Derivative-free optimization: a review of algorithms and comparison of software implementations," J. Glob. Optim. **56**, 1247–1293 (2013).

1. Introduction

The alignment of optical components is crucial for the assembly of optical systems in order to ensure certain performance criteria. Examples for such optical systems range from lithographic equipment [1] to interferometers [2, 3], and fourier-transform infrared spectrometers [4]. Small alignment deviations can lead to wavefront errors that can significantly impact the performance of such devices or even render them entirely useless. To date, the vast majority of commercial optical systems are assembled by employing passive alignment approaches. Therein, optical components are equipped with passive adjustment mechanisms and are manually fine-adjusted via heuristic approaches [5, 6]. This, in turn, leads to high labor cost and increased production cost as well as increased manufacturing time. Therefore, ongoing research concentrates on active (also: automatic) alignment approaches that utilize computer-aided feedback and active driving mechanisms [7–10].

Inferring optical component positions solely from detector measurements is a challenging task. This identification process requires (at least partial) knowledge of the underlying model of the optical system. For systems with simple components (spheric, rotationally symmetric lenses with large radii where decentration is negligible) one can utilize analytic models (such as the extended ray-transfer matrix) [11, 12] for the evaluation of misalignments but for more complex systems or systems with non-negligible decentration one has to resort to full numerical ray-tracing simulations. Supervised learning techniques such as neural networks are able to provide a model-free approach to identify misalignments [13].

Feedback for the identification process can be either intensity-based by employing a CCD camera [14–16] or wavefront-based [17] by employing a (Shack-Hartmann) wavefront sensor. Linear identification techniques compute the Jacobian of the wavefront deviation w.r.t. position deviations. The positions of the components can then be retrieved by utilizing the pseudoinverse of the Jacobian. However, the pseudoinverse is often ill-conditioned and therefore amplifies measurement noise. Furthermore, this limited approach is only valid within a small region around the linearization point and does not consider axes-coupling [18, 19]. A nonlinear approach to the

identification problem consists of constructing a merit function that needs to be minimized in order to yield the respective optical component positions [20–22]. The corresponding optimization problem can be minimized by standard derivative-free optimization algorithms. A dynamic approach for the identification is to use Kalman filtering techniques [16, 17]. For the alignment of interfering beams, differential wavefront sensing became popular which senses phase differences within a quadrant photo diode [23–25].

While several work flows have been proposed for the active alignment in assembly processes [25, 26], our presented approach offers a tight integration of simulation and experimental data. This is done by utilizing identification techniques in order to update a simulation model that runs in parallel with the assembly process. This yields a systematic approach enabling the possibility of assessing predicted wavefront errors and therefore process-integrated conformance testing. These can be used in order to correct either the simulation model or the real physical positions of the optical components during the assembly process. The key contributions of this paper can be summarized as:

- Presentation of a predictor-corrector framework for the systematic alignment of optical components during assembly processes

- Presentation of a hybrid optical model including novel notation

- Simultaneous model adaptation by identification and virtual wavefront prediction during the assembly process

- Correction of virtual or real positions of optical components during the assembly process based on future tolerance assessment (conformance testing)

The proposed framework can be applied e.g. to small series production of optical systems. For large scale productions it is economically sustainable to intensively quantify the system including all tolerances on all optical parameters before deploying production. For small series production, however, the cost-benefit ratio is higher due to smaller quantities and thus a lower revenue. Here, the proposed predictor-corrector framework can give insight by predicting the wavefront and correcting components during the assembly which facilitates custom production without cost-intensive tolerance analysis beforehand. Furthermore, positioning systems for optical system are highly specialized and expensive tools. By lowering the tolerances it is possible to utilize a more generic and cheaper positioning system.

This paper is organized as follows. Sec. 2 presents the proposed predictor-corrector framework and outlines its notation and work flow. Sec. 3 provides experimental validation of our presented predictor-corrector framework by utilizing a beam expander as demonstrator. Sec. 4 concludes the paper with a short summary and future work.

2. Predictor-corrector framework

In this section we will present the predictor-corrector framework and its fundamental concepts. For this, the underlying hybrid model and its corresponding notation is subsequently outlined. Afterwards, the process flow and its core components are described in more detail.

2.1. Notation for hybrid model

In this paper, we consider optical systems with serial topology (i.e. no beam splitting) consisting of n static optical components. A light source ($i=0$) and a detector ($i=n+1$) are placed in the optical train as first and last component, respectively. These components will be considered fixed without loss of generality throughout the remainder of this paper.

Before assembling an optical system, a nominal optical system is given by an initial optical design laid out to satisfy certain desired requirements (e.g. maximum allowable wavefront error

tolerance). Each optical component is then assigned a (virtual) position $\mathbf{x}_{S,i} \in \mathbb{R}^{n_d}$ for $i = 1, ..., n$ from the simulation which is pre-determined by the nominal design. Therein, n_d denotes the degrees of freedom of the optical component. If no positioning uncertainties and tolerances were present, the assembly process would yield the nominal design. However, since such uncertainties are non-negligible in real-world assembly processes, the actual positions deviate from the nominal positions. Therefore, we can similarly define actual optical component positions $\mathbf{x}_i^* \in \mathbb{R}^{n_d}$ for $i = 1, ..., n$ that adhere to the real system. These actual positions can be found by means of identification (see Sec. 2.3).

By making this distinction between virtual and actual positions, we can define a hybrid model that comprises both quantities. For every assembly step i, the i-th component is identified while the remaining $n - i$ components are virtual and are to be added in the upcoming assembly steps. For better readability, we can define a set of identified positions $\mathbf{X}_i^* \in \mathbb{R}^{n_d \times i}$ by

$$\mathbf{X}_i^* := (\mathbf{x}_1^*, ..., \mathbf{x}_i^*)$$

and a set of virtual positions $\mathbf{X}_{S,i} \in \mathbb{R}^{n_d \times (n-i)}$ by

$$\mathbf{X}_{S,i} := (\mathbf{x}_{S,i+1}, ..., \mathbf{x}_{S,n}).$$

The combination yields a set of hybrid positions $\mathbf{X}_{H,i} \in \mathbb{R}^{n_d \times n}$ defined as

$$\mathbf{X}_{H,i} := (\mathbf{X}_i^*, \mathbf{X}_{S,i})$$

for each assembly step $i = 0, ..., n$. Two special cases arise for

    (i) $i = 0$ where the hybrid model degenerates to the nominal (completely virtual) design $\mathbf{X}_{H,0} := (\mathbf{X}_0^*, \mathbf{X}_{S,0}) = \mathbf{X}_{S,0}$, and

    (ii) $i = n$ where the hybrid model degenerates to the (completely assembled) identified optical system $\mathbf{X}_{H,n} := (\mathbf{X}_n^*, \mathbf{X}_{S,n}) = \mathbf{X}_n^*$.

2.2. Work flow of the predictor-corrector framework

The presented predictor-corrector framework consists of a discrete work flow. The framework is briefly outlined here for the i-th assembly step and the core steps are described in more detail in Sec. 2.3-2.5. In this paper, we choose to encode the wavefront in form of Zernike coefficients $\mathbf{z} \in \mathbb{R}^{n_z}$ which are obtained after mapping the positions of optical components by the nonlinear function $h : \mathbb{R}^{n \times n_d} \to \mathbb{R}^{n_z}$ as

$$\mathbf{z} = h(\mathbf{X}). \tag{1}$$

They are by default referenced to the detector coordinate frame in this paper. It should be noted that the presented framework works independently from the chosen wavefront representation. Since we consider only static optical components, the wavefront and therefore the coefficients are solely dependent on their positions without being time-dependent. Figure 1 depicts the proposed work flow of the predictor-corrector framework which can be summarized as follows:

    1. Placement of optical component
        The i-th optical component is brought into the optical train by virtual insertion into the simulation model and simultaneous physical insertion into the real system by a positioning system. The desired position of the i-th lens is given by $\mathbf{X}_{H,i-1}^n$ of the previous assembly step/initial optical system design. It should be noted that the positioning of the optical component is subject to uncertainty (due to limited positioning accuracy) and the actual placement corresponds to a draw from a probability distribution.
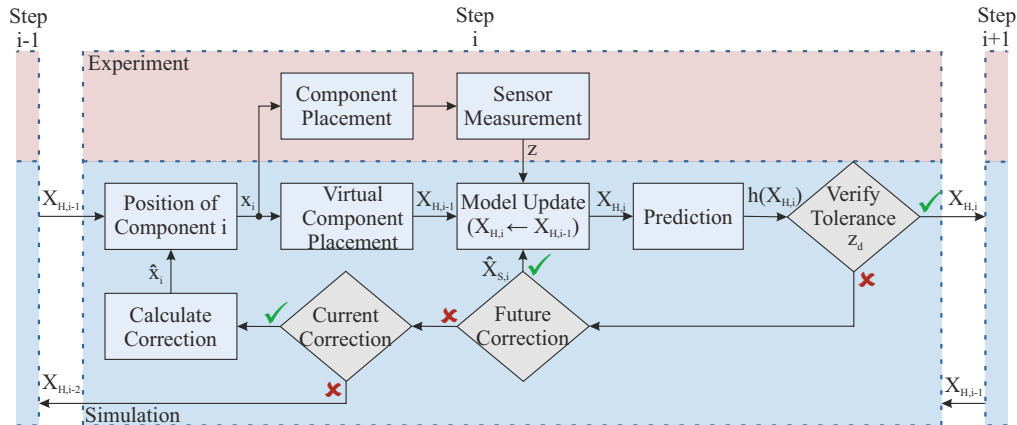
Fig. 1. Flow diagram of the proposed predictor-corrector framework.

2. Sensor measurements
   After the optical component i has been inserted, real measurements $\mathbf{z}$ from the wavefront sensor can be obtained.

3. Model update
   The obtained sensor measurements $\mathbf{z}$ can be used to update the virtual position $\mathbf{x}_{S,i}$ to conform to the real position $\mathbf{x}_i^*$ (**model identification step**) which leads to an update of the hybrid set $\mathbf{X}_{H,i} \leftarrow \mathbf{X}_{H,i-1}$. This step will be described in more detail in Sec. 2.3.

4. Prediction
   Virtual completion of the model allows for a prediction of the wavefront at the detector given the hybrid set $\mathbf{X}_{H,i}$ (**prediction step**) which yields the wavefront if all remaining components would be placed according to their nominal positions (i.e. no positioning errors).

5. Conformance testing and correction calculation
   In this step, the predicted wavefront from the previous step can be assessed by choosing an appropriate metric. If tolerance criteria from the previous step are not met, the virtual or real system needs to be altered accordingly (**conformance testing & correction step**). There are three options to do so:

   (I) Future correction: Correct error in the virtual model by re-alignment of optical components to be assembled

   (II) Current correction: Correct position of current optical component by calculation of a positional correction term and applying it to the system. If multiple such iterations are required during a configuration, these will be called cycles thereafter.

   (III) Past correction: Correct error by going one step back in the assembly procedure and correct previous optical component position.

2.3. Model identification step

The model identification step consists of solving the inverse problem of the mapping (1). Given a wavefront measurement, the goal is to retrieve the position(s) of the current optical component(s) $\mathbf{x} \in \mathbf{X}$ by

$$\mathbf{X} = h^{-1}(\mathbf{z}). \qquad (2)$$

In this paper we follow a nonlinear approach to solve (2). This can be realized by an optimization problem with a nonlinear merit function J [20, 22] that is minimized w.r.t. the current component position

$$\mathbf{x}^* = \arg\min_{\mathbf{x} \in \mathbf{X}} J(\mathbf{X}, \mathbf{z}) \tag{3}$$

with weighted quadratic merit function

$$J(\mathbf{X}, \mathbf{z}) = \|\mathbf{z} - h(\mathbf{X})\|_{\mathbf{W}} = \sqrt{(\mathbf{z} - h(\mathbf{X}))^T \mathbf{W} (\mathbf{z} - h(\mathbf{X}))}. \tag{4}$$

The weights incorporated in the diagonal weighting matrix $\mathbf{W} = \mathrm{diag}(w_1, ..., w_{n_z})$ can be used for example to discount the influence of higher-order aberrations. Solving (3)-(4) can be realized by any derivative-free optimization algorithm (Levenberg-Marquardt, Nelder-Mead, Particle Swarm, Genetic Algorithms, Damped Least-Squares etc.). The interested reader is referred to [27] for a recent comparative study on such solvers.

2.4. Prediction step

This step consists of a simple forward simulation based on the identified and virtual component positions. A single simulation $\mathbf{z}_p = h(\mathbf{X}_{H,i})$ is executed to predict the wavefront at the detector based on the hybrid set.

2.5. Conformance testing and correction step

In this step, the predicted wavefront error of the optical system given the hybrid set $\mathbf{X}_{H,i}$ can be assessed by choosing an appropriate metric (typically, root-mean-square error (RMS) or peak-to-valley (PV)). In this paper, we chose the wavefront deviation expressed as the weighted norm of Zernike coefficient differences (weighted RMS) at the detector to be below a certain tolerance

$$\|\mathbf{z}_d - \mathbf{z}_p\|_W = \|\mathbf{z}_d - h(\mathbf{X}_i^*, \mathbf{X}_{S,i})\|_W \leq \mathrm{TOL}. \tag{5}$$

Therein, $\mathbf{z}_d$ are the Zernike coefficients corresponding to a desired wavefront which should be achieved at the completion of the predictor-corrector framework and are specified by the initial optical design (see Sec. 2.1). If (5) holds, the next assembly step can be executed. If not, corrective measures need to be taken. In order to avoid physical assembly/correction steps we prioritize virtual position corrections on the future components to be assembled. If this is not possible, a correction of the current component should occur which may not yet be fixed and therefore can easily be manipulated. If this step is not feasible, a step back in the assembly process needs to be made. The three correction options can be formalized as:

(I) Future correction
An optimization problem similar to the identification step needs to be solved

$$\hat{\mathbf{X}}_{S,i} = \arg\min_{\mathbf{X}_{S,i} \subset \mathbf{X}_{H,i}} J(\mathbf{X}_{H,i}, \mathbf{z}_d).$$

However, here we keep the real components fixed and only optimize over all remaining virtual components. The outcome allows to reassess the tolerance specification (5) with updated virtual positions by

$$\|\mathbf{z}_d - h(\mathbf{X}_i^*, \hat{\mathbf{X}}_{S,i})\|_W \leq \mathrm{TOL}. \tag{6}$$

If (6) holds we can update the simulation model and execute next assembly step. It should be noted that this step potentially incurs a high computational load if the remaining number of optical components is large since the search space increases exponentially with the number of components. This can be mitigated by

- Reducing the prediction horizon by limiting the number of components to be considered in the future correction step
- Reducing the adjustment DOF for the remaining components

(II) Current correction

If both (5) and (6) are violated, we try to change the component of the current assembly step. This leads to an optimization problem over the current optical component

$$\hat{\mathbf{x}}_i = \underset{\mathbf{x}_i \in \mathbf{X}_{H,i}}{\arg \min} J(\mathbf{X}_{H,i}, \mathbf{z}_d).$$

Again, the predicted tolerance can be reassessed by

$$\|\mathbf{z}_d - h(\mathbf{X}_{i-1}^*, \hat{\mathbf{x}}_i, \mathbf{X}_{S,i})\|_W \leq \text{TOL}. \tag{7}$$

If (7) holds, we reiterate the first step of the current cycle (placement of optical component) with the updated current optical component position $\hat{\mathbf{x}}_i$.

(III) Past correction

If (5), (6) and (7) are violated, the current optical component needs to be removed and the error needs to be corrected by going one step back in the assembly procedure.

In conclusion to this section, the proposed predictor-corrector framework is shown in Alg. 1. If TOL is chosen too low, the framework (see Fig. 1) might get stuck in an infinite loop. To address this issue, we introduce an additional iteration counter $iter$ that is incremented for each physical correction. The algorithm will then terminate after a user-specified maximum iteration $iter_{max}$ has been exceeded.

3. Experimental verification with beam expander

In order to verify the presented predictor-corrector framework, a beam expander (as exemplary demonstrator) is assembled. While the proposed framework is intended for all optical systems where the individual optical components can be modeled with sufficient accuracy, a simple two-lens system is analyzed hereafter.

3.1. Experimental setup

The experimental setup (see Fig. 2(a)) consists of a laser ($\lambda = 532$ nm) followed by an adjustable neutral-density filter in order to prevent sensor damage at different configurations. For beam shaping, two bi-convex NBK-7 lenses with 50 mm and 100 mm focal length are used in the experiments, respectively. Each lens is mounted inside a tip-tilt stage with 15° travel at 1 °/rev resolution. Furthermore, these are mounted on top of XYZ stages with a maximum travel of ±2 mm with a fine resolution of ±300 μm. The rigid interconnection of these stages results in a 5-DOF stage for each lens. These positioning stages are equipped with metric taps which can be used to alter the position/orientation according to the calculations made by the predictor-corrector framework. A Shack-Hartmann Wavefront Sensor (Thorlabs WFS150-5C with a 150 μm microlens array pitch) is placed at the end of the optical train. The fitting pupil for obtaining the Zernike coefficients with constant diameter of 3 mm is centered w.r.t. the CCD sensor (4.2×4.2 mm²). The diameter has been chosen to sufficiently capture enough emitted laser light for all feasible position combinations with the employed 5-DOF stages such that a Zernike fitting process is always possible at the model identification steps. Furthermore, the wavefront sensor is equipped with an additional extension tube including a 532 nm bandpass filter to mitigate the impact of ambient light and therefore reduce measurement noise.

For simulations, the well-known ray tracing software ZEMAX OpticStudio (in sequential mode) is used and called via MATLAB. The beam divergence is accounted for in the simulation model.

Algorithm 1 Predictor-Corrector Framework (PCF)

procedure PCF($\mathbf{X}_{S,0}, \mathbf{z}_d, iter_{max}$, TOL)
$\quad i = 1, \mathbf{X}_{H,0} \leftarrow \mathbf{X}_{S,0}, iter = 0$
$\quad$ **while** $i \leq n \wedge iter \leq iter_{max}$ **do**
$\qquad$ Placement of virtual and real optical component in optical train at $\mathbf{x}_i \in \mathbf{X}_{H,i-1}$
$\qquad$ Obtain wavefront sensor measurement $\mathbf{z}$
$\qquad \mathbf{x}_i^* = \arg\min_{\mathbf{x}_i} J(\mathbf{X}_{H,i-1}, \mathbf{z})$ $\qquad\qquad\qquad$ ▷ Model Identification
$\qquad \mathbf{X}_{H,i} \leftarrow (\mathbf{X}_{i-1}^*, \mathbf{x}_i^*, \mathbf{X}_{S,i}), \mathbf{z}_p \leftarrow h(\mathbf{X}_{H,i})$ $\qquad$ ▷ Update & Predict
$\qquad$ **if** $\|\mathbf{z}_d - \mathbf{z}_p\|_W >$ TOL **then** $\qquad\qquad\qquad$ ▷ Tolerance Verification
$\qquad\quad \hat{\mathbf{X}}_{S,i} = \arg\min_{\mathbf{X}_{S,i}} J(\mathbf{X}_{H,i}, \mathbf{z}_d)$ $\qquad\qquad$ ▷ Future Correction
$\qquad\quad \mathbf{X}_{H,i} \leftarrow (\mathbf{X}_i^*, \hat{\mathbf{X}}_{S,i}), \mathbf{z}_p \leftarrow h(\mathbf{X}_{H,i})$ $\qquad$ ▷ Update & Predict
$\qquad\quad$ **if** $\|\mathbf{z}_d - \mathbf{z}_p\|_W >$ TOL **then** $\qquad\qquad$ ▷ Tolerance Verification
$\qquad\qquad \hat{\mathbf{x}}_i = \arg\min_{\mathbf{x}_i} J(\mathbf{X}_{H,i}, \mathbf{z}_d)$ $\qquad\qquad$ ▷ Current Correction
$\qquad\qquad \mathbf{X}_{H,i-1} \leftarrow (\mathbf{X}_{i-1}^*, \hat{\mathbf{x}}_i, \mathbf{X}_{S,i}), \mathbf{z}_p \leftarrow h(\mathbf{X}_{H,i})$ $\qquad$ ▷ Update & Predict
$\qquad\qquad$ **if** $\|\mathbf{z}_d - \mathbf{z}_p\|_W >$ TOL **then** $\qquad$ ▷ Tolerance Verification
$\qquad\qquad\quad \mathbf{X}_{H,i-2} \leftarrow \mathbf{X}_{H,i-1}$
$\qquad\qquad\quad i \leftarrow i - 1$ $\qquad\qquad\qquad\qquad$ ▷ Return to Previous Assembly Step
$\qquad\qquad$ **else**
$\qquad\qquad\quad i \leftarrow i, iter \leftarrow iter + 1$ $\qquad\qquad$ ▷ Try Correction & Increment Counter
$\qquad\qquad$ **end if**
$\qquad\quad$ **else**
$\qquad\qquad i \leftarrow i + 1$ $\qquad\qquad\qquad\qquad\qquad$ ▷ Proceed to Next Assembly Step
$\qquad\quad$ **end if**
$\qquad$ **else**
$\qquad\quad i \leftarrow i + 1$ $\qquad\qquad\qquad\qquad\qquad$ ▷ Proceed to Next Assembly Step
$\qquad$ **end if**
$\quad$ **end while**
$\quad$ **return** $\mathbf{X}_n^* = \mathbf{X}_{H,n}$ $\qquad\qquad\qquad$ ▷ Assembled and Identified Optical System
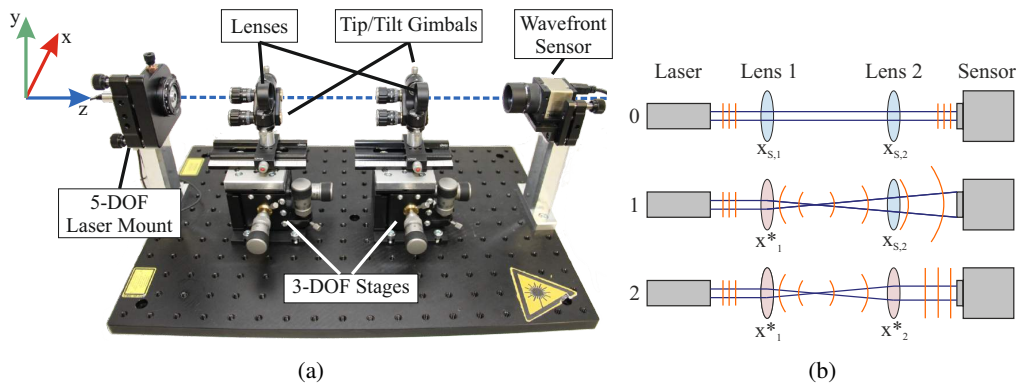**end procedure**

Fig. 2. Experimental beam expander setup (a, ND filter not depicted) and schematic depiction of the three configurations (0,1,2) during the beam expander assembly process (b).

3.2. General description of beam expander experiments

Since the optical system consists of two optical components, there are three possible configurations. Configuration 0 represents the initial phase before any optical element has been placed,

configuration 1 represents the configuration with the first lens inserted, and configuration 2 represents the phase where both optical elements have been inserted into the optical train, see Fig. 2(b). For the optimization problem (3)-(4), we will use the first $n_z = 10$ normalized Zernike standard polynomials (see Tab. 1) given in waves and choose $\mathbf{W}$ as a truncated diagonal identity matrix that dismisses piston and uniformly weights higher-order coefficients since we do not prefer a certain aberration to be compensated. The Nelder-Mead algorithm will be chosen as

Table 1. Utilized Zernike standard polynomials with corresponding coefficients.

Zernike coefficients z_i	Normalization factor	Zernike standard polynomials $Z_i(\rho, \theta)$
z_1	1	1
z_2	2	$\rho \cos(\theta)$
z_3	2	$\rho \sin(\theta)$
z_4	$\sqrt{3}$	$2\rho^2 - 1$
z_5	$\sqrt{6}$	$\rho^2 \sin(2\theta)$
z_6	$\sqrt{6}$	$\rho^2 \cos(2\theta)$
z_7	$2\sqrt{2}$	$(3\rho^3 - 2\rho) \sin(\theta)$
z_8	$2\sqrt{2}$	$(3\rho^3 - 2\rho) \cos(\theta)$
z_9	$2\sqrt{2}$	$\rho^3 \sin(3\theta)$
z_{10}	$2\sqrt{2}$	$\rho^3 \cos(3\theta)$

optimization algorithm. Initially, laser and detector are manually aligned and calibrated such that a planar wavefront is detected by the wavefront sensor. The stages and gimbals, however, are not pre-adjusted and are subject to alignment tolerances. The following optical systems are to be assembled (initial optical design):

- Experiment (a): Lens 1 and 2 at "zero" position, desired wavefront with coefficients $\mathbf{z}_d = (0, ..., 0)$ and weighted RMS tolerance given by TOL = $\lambda/7$.

- Experiment (b): Lens 1 at "zero" position and lens 2 tilted by 5° around the y-axis which leads to a desired wavefront with coefficients $\mathbf{z}_d = (0, 1.52, 0, ..., 0)$ and weighted RMS tolerance given by TOL = $\lambda/3$.

The maximum iteration counter is set to five ($iter_{max} = 5$).

3.3. Experimental results

Tab. 3 shows the results for the experiments (a) and (b) with hybrid lens positions according to Sec. 2. The lens positions are given w.r.t. their respective nominal coordinate system from CAD design. The predicted cost is evaluated according to (4) as $J(\mathbf{X}, \mathbf{z}_d)$ where $\mathbf{X}$ are positions given by the first and second lens in the respective columns. Due to the spherical aberration caused by the spherical lenses, the initial predicted cost is non-zero. The correction steps are applied to the lenses with the help of the Cartesian stages and tip/tilt gimbals according to $\mathbf{x}_c = \mathbf{x}^* - \hat{\mathbf{x}}$ during a cycle.

In experiment (a), the tolerance on the predicted cost is violated in the first configuration after the model update step which results in $\mathbf{X}_{H,1} = (\mathbf{x}_1^*, \mathbf{x}_{S,2})$. Fig. 3 shows the corresponding identification procedure (selected Zernike coefficients of this are given in Tab. 2) and Fig. 4(a) the wavefront measurement. The correction step leading to $\mathbf{X}_{H,1} = (\mathbf{x}_1^*, \hat{\mathbf{x}}_{S,2})$ shows how a change in the second lens position results in a predicted cost below the desired tolerance threshold (c.f. Fig. 4(b) for the predicted and corrected wavefront). The correction is applied to the system and the following model update step (resulting in $\mathbf{X}_{H,2} = (\mathbf{x}_1^*, \mathbf{x}_2^*)$ with utilized wavefront measurement seen in Fig. 4(c)) again shows a violation on the tolerance of the predicted cost. This can be rectified by the correction in the second cycle (see $\mathbf{X}_{H,2} = (\mathbf{x}_1^*, \hat{\mathbf{x}}_2)$ and Fig. 4(d) for the predicted
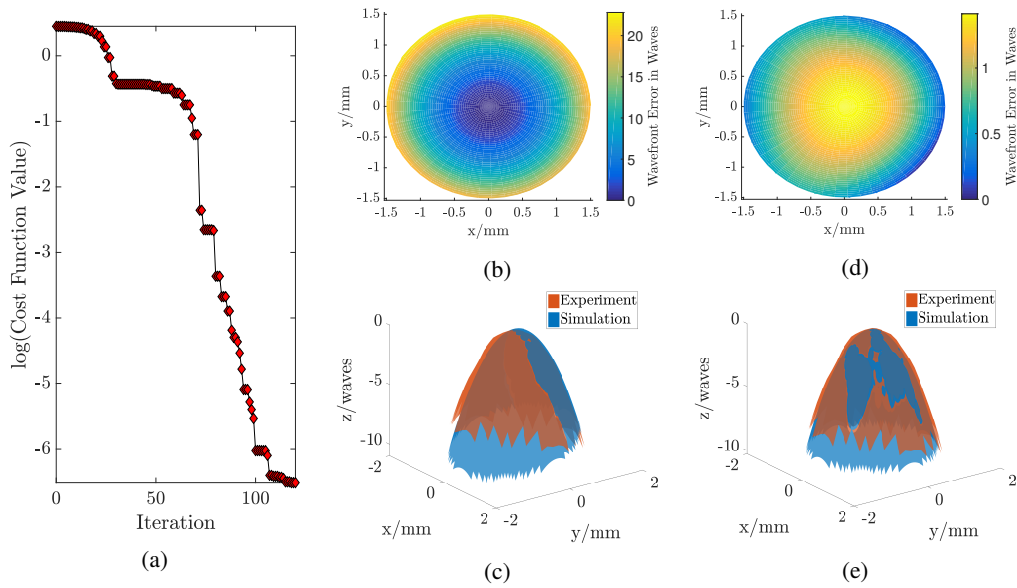
(b)

(d)

(a)

(c)

(e)

Fig. 3. Identification step (model update) in first assembly step of experiment (a): Iteration of cost function value (a) and corresponding predicted wavefront deviation (reconstructed from Zernike coefficient error) and simulated/obtained wavefront at iteration 0 (maximum wavefront error 22.83 waves) (b)-(c) and iteration 120 (maximum wavefront error 1.41 waves) (d)-(e). A selection of corresponding Zernike coefficients for this identification process are given in Tab. 2

and corrected wavefront). Another identification step (see $\mathbf{X}_{H,2} = (\mathbf{x}_1^*, \mathbf{x}_2^*)$ and Fig. 4(e)) shows that the desired tolerance is met after applying the correction.

The results of experiment (b) are similar, except that the first model update phase shows that the predicted cost is kept below the user-defined tolerance.

In this demonstrator, the changes in the wavefront are more sensitive to despace/decentration than to tip/tilt which leads to relatively high errors for identified tip/tilt values. This becomes evident when performing a sensitivity analysis for both configurations. Linearization of (1) leads to $\delta \mathbf{z} = S_i \cdot \delta \mathbf{x}_i$, where S_i is the sensitivity matrix for the i-th configuration w.r.t. $\mathbf{x}_i$. For our demonstrator, these sensitivity matrices are

$$
S_1 = \begin{pmatrix}
0 & 0 & 0 & 0 & -0.12 \\
-33.51 & 0 & 0 & -2.05 & 0 \\
0 & -33.51 & 2.05 & 0 & 0 \\
0 & 0 & 0 & 0 & -0.07 \\
0 & 0 & 0 & 0 & 0 \\
0 & 0 & 0 & 0 & 0 \\
0 & 0 & 0 & 0 & 0 \\
0 & 0 & 0 & 0 & 0 \\
0 & 0 & 0 & 0 & 0
\end{pmatrix}
\text{and } S_2 = \begin{pmatrix}
0 & 0 & 0 & 0 & 0.57 \\
75.63 & 0 & 0 & 1.58 & 0 \\
0 & 75.63 & -1.58 & 0 & 0 \\
0 & 0 & 0 & 0 & 0.33 \\
0 & 0 & 0 & 0 & 0 \\
0 & 0.02 & -0.01 & 0 & 0 \\
0.02 & 0 & 0 & 0.01 & 0 \\
0 & 0 & 0 & 0 & 0 \\
0 & 0 & 0 & 0 & 0
\end{pmatrix}.
\tag{8}
$$

This also shows that the inclusion of higher-order polynomials will not increase accuracy in the optimization phases (identification/correction calculation) for this demonstrator.

However, at the completion of the predictor-corrector framework the desired wavefront is achieved (which is essential in assembling optical systems) even if values do not perfectly correspond to real values. It should be noted that we only care about achieving a desired wavefront and not absolute positioning precision of each optical component.

Table 2. Iteration of first four Zernike coefficients (in waves) at selected iterations (1, 5, 10, 50, 80, 120) during the first identification step in experiment (a). The remaining Zernike coefficients (z_5 - z_{10}) are zero since they do not influence the wavefront (see sensitivity matrix S_1 from (8)).

$\mathbf{z}_d$	$^1\mathbf{z}$	$^5\mathbf{z}$	$^{10}\mathbf{z}$	$^{50}\mathbf{z}$	$^{80}\mathbf{z}$	$^{120}\mathbf{z}$
1.8100	-4.7952	-4.7952	-4.7952	-4.7948	-4.7950	-4.7951
0.1190	0	0.0009	0.0025	0.3576	0.1760	0.1189
0.6950	0	-0.0013	-0.0060	-0.5332	-0.7160	-0.6949
-2.7684	-2.7685	-2.7685	-2.7685	-2.7683	-2.7684	-2.7684

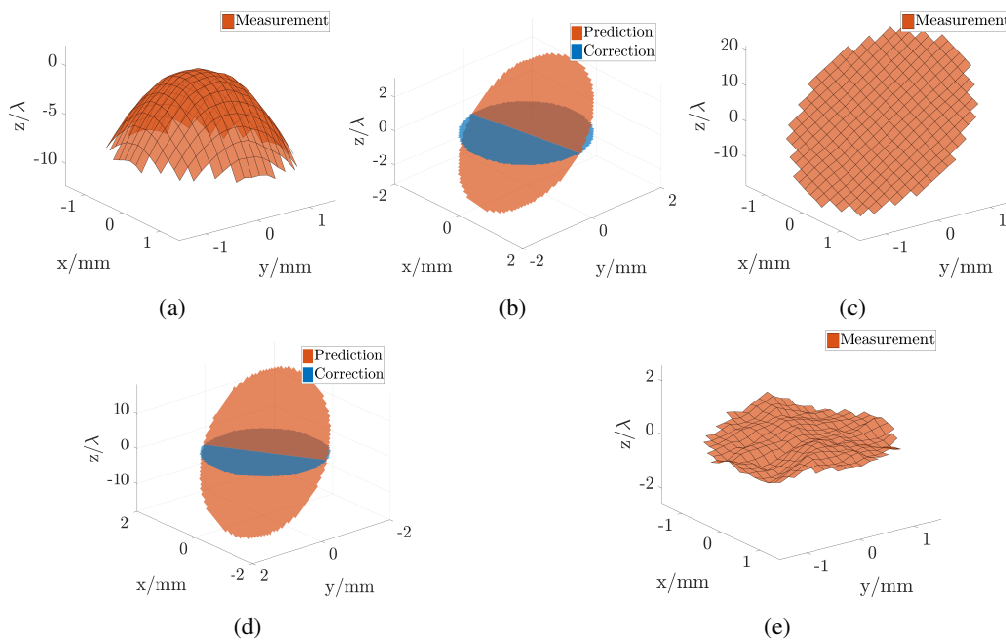Fig. 4. Two consecutive predictor-corrector cycles in experiment (a): Measured wavefront in configuration 1 (a) followed by the predicted and subsequently corrected wavefront in simulation (b). The same is done in the second assembly step where a wavefront is obtained (c), and subsequent prediction-correction simulation calculations (d). The wavefront of the assembled beam expander is shown in (e).

Table 3. Iterative assembly process for the beam expander in experiment (a) and (b). Values for lens positions provided by initial design / simulation (blue) and values provided by identification (red). The corresponding predicted cost (green if below tolerance, red if above tolerance) is shown below.

		Experiment (a)					
		$\mathbf{X}_{H,0}=$ $(\mathbf{x}_{S,1},\mathbf{x}_{S,2})$	$\mathbf{X}_{H,1} =$ $(\mathbf{x}_1^*,\mathbf{x}_{S,2})$	$\mathbf{X}_{H,1} =$ $(\mathbf{x}_1^*,\hat{\mathbf{x}}_{S,2})$	$\mathbf{X}_{H,2} =$ $(\mathbf{x}_1^*,\mathbf{x}_2^*)$	$\mathbf{X}_{H,2} =$ $(\mathbf{x}_1^*,\hat{\mathbf{x}}_2)$	$\mathbf{X}_{H,2} =$ $(\mathbf{x}_1^*,\mathbf{x}_2^*)$
Configuration		0	1		2		
Lens 1	x/mm	0	-1.36E-2	-1.36E-2	-1.36E-2	-1.36E-2	-1.36E-2
	y/mm	0	1.14E-1	1.14E-1	1.14E-1	1.14E-1	1.14E-1
	z/mm	0	-7.21E-3	-7.21E-3	-7.21E-3	-7.21E-3	-7.21E-3
	θ_x/°	0	6.18E-2	6.18E-2	6.18E-2	6.18E-2	6.18E-2
	θ_y/°	0	8.67E-2	8.67E-2	8.67E-2	8.67E-2	8.67E-2
Lens 2	x/mm	0	0	-1.64E-2	-3.60E-1	-5.20E-2	-0.22
	y/mm	0	0	1.10E-1	6.34E-1	8.55E-2	-5.68E-2
	z/mm	0	0	-1.44E-3	1.41E-2	1.04E-2	1.10E-2
	θ_x/°	0	0	-7.72E-2	-6.37E-1	-1.11	-1.10
	θ_y/°	0	0	1.10E-1	8.27E-1	1.60	1.54
Pred. Cost	J/λ	1.9E-03	1.56	1.50E-3	8.94	7.66E-3	1.10E-1

		Experiment (b)					
		$\mathbf{X}_{H,0}=$ $(\mathbf{x}_{S,1},\mathbf{x}_{S,2})$	$\mathbf{X}_{H,1} =$ $(\mathbf{x}_1^*,\mathbf{x}_{S,2})$	$\mathbf{X}_{H,1} =$ $(\mathbf{x}_1^*,\hat{\mathbf{x}}_{S,2})$	$\mathbf{X}_{H,2} =$ $(\mathbf{x}_1^*,\mathbf{x}_2^*)$	$\mathbf{X}_{H,2} =$ $(\mathbf{x}_1^*,\hat{\mathbf{x}}_2)$	$\mathbf{X}_{H,2} =$ $(\mathbf{x}_1^*,\mathbf{x}_2^*)$
Configuration		0	1		2		
Lens 1	x/mm	0	2.91E-3	2.91E-3	2.91E-3	2.91E-3	2.91E-3
	y/mm	0	4.03E-3	4.03E-3	4.03E-3	4.03E-3	4.03E-3
	z/mm	0	-2.60E-3	-2.60E-3	-2.60E-3	-2.60E-3	-2.60E-3
	θ_x/°	0	-1.80E-3	-1.80E-3	-1.80E-3	-1.80E-3	-1.80E-3
	θ_y/°	0	-9.17E-4	-9.17E-4	-9.17E-4	-9.17E-4	-9.17E-4
Lens 2	x/mm	0	0	0	-6.39E-2	1.48E-1	3.75E-1
	y/mm	0	0	0	1.16E-1	3.46E-3	-5.89E-3
	z/mm	0	0	0	-2.47E-1	-5.01E-2	-3.46
	θ_x/°	0	0	0	-2.94E-2	-2.98E-2	-5.37E-1
	θ_y/°	5	5	5	-3.96E-1	-1.84	7.135
Pred. Cost	J/λ	5.42E-2	8.63E-2	8.63E-2	3.04	4.19E-3	2.52E-1

4. Conclusion and future work

In this paper we have presented a predictor-corrector framework for the sequential assembly of optical systems. For this, a hybrid model (including novel notation) has been introduced which allows for a prediction of the future wavefront during the assembly process. With a metric-based assessment of the predicted wavefront error, appropriate correction measures can be taken during the assembly process. This is done by corrections of future virtual components to be assembled, the current optical component, or going one step back in the assembly process. In general, virtual corrections are preferred over actual corrections in order to minimize production time and cost. The proposed approach has been validated utilizing a beam expander for two different nominal lens configurations. Both experiments lead to a wavefront that is below a given wavefront error tolerance at the completion of the predictor-corrector work flow. Tip/tilt values deviate from actual values due to higher sensitivity in translational directions which is a problem inherent to the chosen demonstrator and model identification algorithm.

Future work will consider more complex systems (multiple and diverse optical components as well as underlying parallel topology). For optical systems with less adjustment DOF for each component, the presented approach can be utilized to investigate the benefits of adding additional adjustment DOF to certain optical components in order to increase performance during its assembly. For this, a distinction between physical DOF and virtual DOF could be made. Efficiently searching a large optimization space in the future correction step when an optical system has many optical components can be addressed by employing dimensional reduction strategies such as principal component analysis. Furthermore, the nonlinear optimization can be replaced by a filtering techniques in order to improve accuracy in the model identification step. This will potentially reduce the number of cycles within an assembly step and improve overall model accuracy.